Standardization of Preclinical PET/CT Imaging to Improve Quantitative Accuracy, Precision, and Reproducibility

Journal of Nuclear Medicine, published on September 27, 2019 as doi:10.2967/jnumed.119.231308

Standardization of preclinical PET/CT imaging to improve quantitative accuracy, precision and reproducibility: a multi-center study

Authors

Wendy McDougald[1,2], Christian Vanhove[3], Adrienne Lehnert[4], Barbara Lewellen[4], John Wright[5], Marco Mingarelli[6], Carlos Alcaide Corral[1,2]Jurgen E. Schneider[5], Sven Plein[5], David Newby[1], Andy Welch[6], Robert Miyaoka[4], Stefaan Vandenberghe[3], Adriana Alexandre S. Tavares[1,2]

1. BHF-Centre for Cardiovascular Science, College of Medicine & Veterinary Medicine, University of Edinburgh, UK

2. Edinburgh Preclinical Imaging (EPI), Edinburgh Imaging, University of Edinburgh, UK

3. Department of Electronics and Information Systems, MEDISIP, Ghent University, Belgium

4. Department of Radiology, Imaging Research Laboratory, University of Washington, USA

5. Leeds Institute of Cardiovascular and Metabolic Medicine, Department of Biomedical Imaging Science, LIGHT Laboratories, University of Leeds, UK

6. Aberdeen Biomedical Imaging Centre, School of Medicine, Medical Sciences & Nutrition, University of Aberdeen, UK

Corresponding Author and First Author:

Wendy A McDougald, MScR

University of Edinburgh

Queen's Medical Research Institute, Centre for Cardiovascular Science

47 Little France Crescent

EH16 4TJ

Edinburgh, UK

Phone: 01312426746

Fax: 01312426779

Email: s1575538@sms.ed.ac.uk

Running Title: Preclinical PET/CT standardized protocols

Word count: 6094

Key words: Preclinical PET/CT, Standardization, Hounsfield Units, Absorbed dose, Recovery coefficient

ABSTRACT

Preclinical Positron Emission Tomography/Computed Tomography (PET/CT) is a well-established non-invasive imaging tool for studying disease development/progression and the development of novel radiotracers and pharmaceuticals for clinical applications. Despite this pivotal role, standardization of preclinical PET/CT protocols, including CT absorbed dose guidelines, is essentially non-existent. This study: (1) quantitatively assesses the variability of current preclinical PET/CT acquisition and reconstruction protocols routinely used across multiple centers and scanners; and (2) proposes acquisition and reconstruction PET/CT protocols for standardization of multi-center data, optimized for routine scanning in preclinical PET/CT laboratory. **Methods:** Five different commercial preclinical PET/CT scanners in Europe and USA were enrolled. Seven different PET/CT phantoms were used for evaluating biases on default/general scanner protocols; followed by developing standardized protocols. PET, CT and absorbed dose biases were assessed. **Results:** Site default CT protocols: Greatest extracted Hounsfield Units (HU) for water was 133HU and -967HU for air, significant differences in all tissue equivalent material (TEM) groups were measured. Average CT absorbed dose for mouse and rat was 72mGy and 40mGy, respectively. Standardized CT protocol: Greatest extracted HU for water was -77HU and -990HU for air, TEM precision improved with a reduction in variability for each tissue group. Average CT absorbed dose for mouse and rat was reduced to 37mGy and 24mGy, respectively. Site default PET protocols: Uniformity was substandard in one scanner, Recovery Coefficients (RCs) were either over or under estimated (maximum of 43%), standard uptake values (SUVs) were biased by a maximum of 44%. Standardized PET protocol: Scanner with substandard uniformity improved by 36%, RC variability was reduced by 13% points and SUV accuracy improved to 10%. **Conclusion:** Data revealed important quantitative bias in preclinical PET/CT and absorbed doses with default protocols. Standardized protocols showed improvements in measured PET/CT accuracy and precision with reduced CT absorbed

dose across sites. Adhering to standardized protocols generates reproducible and consistent preclinical imaging datasets, thus augmenting translation of research findings to the clinic.

INTRODUCTION

The necessity for standardization in clinical Positron Emission Tomography/Computed Tomography (PET/CT) protocols was acknowledged and initiated nearly 20 years ago (*1–4*). This recognition mainly stemmed from multi-center trials focused in quantifying and tracking changes in malignant tumors as well as prognosis and treatment evaluations. Today preclinical PET/CT is a pivotal quantitative imaging research tool supporting innovative research in areas such as disease diagnosis, prognosis and in the development of novel radiotracers and pharmaceuticals (*5–10*). Yet, standardization in preclinical PET/CT imaging remains essentially non-existent. To date there is not an established global standard protocol used across preclinical research centers. The lack of preclinical protocol standardization impacts quantitative image analysis, reproducibility and consistency across sites. Thus, limiting reliable translational image data to clinical research and applications.

The preclinical PET/CT community has undertaken efforts towards the development of guidelines regarding animal handling/preparation and scanner quality control testing (*11–17*). Several preclinical studies evaluating PET National Electric Manufactures Association, NEMA NU 4 2008 performance also exist (NEMA performance literature in Supplemental Table 1 (*1-13*). However, not until the present study has establishing preclinical imaging standard protocols been directly addressed and set forth. Additionally, due to unregulated preclinical CT doses absorbed ionized radiation is assessed; fostering the impetus for regulating ionizing absorbed radiation doses (*18*). Regulating CT doses will reduce the cumulative severity effects of radiation. This will minimize animal suffering while reducing the potential impact of biological responses from the radiation effect on research studies, in line with the National Centre for the Replacement, Refinement and Reduction of Animals in Research (NC3Rs).

This study addresses the lack of standardized protocols by assessing quantitative accuracy (known vs measured) and precision (reduced variability) of currently used routine protocols across multiple sites and scanners for the development of standard protocols.

MATERIALS AND METHODS

This multi-center study involved five sites for a total of five different commercial preclinical PET/CT scanners (Bruker Albira, Mediso nanoPET/CT, Sedecal Super Argus, Siemens Inveon and Trifoil LabPET/CT), arbitrarily labelled 1 to 5. First, routine/default (hereon referred to as default) PET and CT protocols were evaluated for image quality and quantification biases using seven commercially available preclinical microPET and microCT phantoms (Supplemental Table 2, labeled A-G). Default protocols were set either by the vendor or the site for their routine use of imaging small animals. Each CT default protocol was also assessed based on measured absorbed ionizing radiation. Secondly, several different PET reconstruction methods were quantitatively analyzed for standardization. Thirdly, standardized CT protocols were determined from the least Hounsfield Units (HU) biases between all imaging data sets. Numerical criteria for biases were based on the parameters in Table 1. Results were then evaluated in the same manner as the default protocols on each scanner. All PET and CT imaging data sets (default and standard) per scanner per phantom and dose measurements were acquired as n=3 for the analysis. No rodents were used in this study, only dedicated PET and CT phantoms. The lead author visited each site multiple times for the image acquisitions and carried out all the data analysis.

Default PET/CT Protocols

PET. PET images were acquired as a single bed position for a duration of 20-minutes, energy windowing of 250 - 700 keV with the phantoms placed at the frontend of the scanner bed, positioned inside the bore at the isocenter, aligning sagittal, axial and coronal planes. An

activity of 10±6 MBq of ^{18}F-FDG in 23 mL of distilled water was injected into a PET image quality (IQ) phantom which includes 5 hots rods 1-5 mm for recovery coefficient (RC), uniformity section and spill-over-ratio (SOR) section composed of 2 cylinders filled with non-radioactive water and air. Whilst, 64±5 MBq of ^{18}F-FDG in 24 mL of distilled water was injected into a PET rod phantom containing 0.6, 0.8, 1.0, 1.2, 1.5 and 2.0 mm rods. The targeted range of activities was selected based on typically reported injected doses into small animals, the design and purpose of the PET phantoms.

Emission data was reconstructed using the sites' default protocols. Protocols are listed by scanner (1-5), method (ordered subset expectation maximization (OSEM) or maximum likelihood expectation maximization (MLEM)), voxel size, filter and matrix size: 1 (2D OSEM 2 iterations 16 subsets, 0.4 mm, Ramp,175x175), 2 (3D OSEM 4 iterations 6 subsets, 0.4 mm, Ramp,108x110), 3 (3D OSEM 2 iterations 18 subsets, 0.3 mm, Hamm, 256x256), 4 (3D MLEM 12 iterations, 0.7 mm, no filter,108x108), and 5 (2D MLEM 50 iterations, 0.5 mm, no filter, 200x200). Scanners 2 and 3 also correct for partial volume effects by incorporating a point spread function (PSF) into the reconstruction algorithm. All scanners apply scatter, normalization and randoms corrections, whereas scanners 1-4 apply attenuation corrections. Scanner 5 allows the user to opt out of using the CT generated attenuation correction maps.

For the PET IQ image analysis, reconstructed data was imported into PMOD version 3.806 (PMOD, Zurich, Switzerland) and a MATLAB software tool implemented by Mediso (Mediso, Hungary). The Mediso MATLAB software program utilizes the NEMA NU 4-2008 standards. The quantitative assessment of the PET included uniformity, RC, SOR and standard uptake values (SUV).

PET Statistical analysis. In accordance to NEMA, using the IQ phantom, uniformity is reported as the percent standard deviation (%STD) from a 22.5mm diameter by 10mm long cylindrical volume of interest (VOI) over the uniform region of the phantom. RC is calculated based on values extracted from regions of interest (ROI) twice the diameter of each hot rod. The

MATLAB program draws linear profiles along the hot rods in the axial direction. The mean pixel values of the linear profiles are divided by the mean pixel value of the uniform region, Equation 1 below (*19*,*20*).

$$RC = \frac{ROI_{rod}}{VOI_{uniformity}} \quad \text{(Eq.1)}$$

ROI rod represents the mean pixel values from the hot rods (1, 2, 3, 4 and 5 mm) and *VOI uniformity* is the mean activity concentration from the uniformity region.

VOIs are drawn on each air and water chamber with SOR values calculated as ratios between the air or water chamber mean value divided by the uniformity mean measurement, Equation 2 (*19*,*20*).

$$SOR = \frac{VOI_{chamber}}{VOI_{uniformity}} \text{ (Eq.2)}$$

VOI chamber represents the mean value from each individual air or water chamber and *VOI uniformity* is the uniformity measurement. Representative images of the Mediso MATLAB software tool for the PET IQ analysis displaying the regions of the IQ phantom (uniformity, RC and SOR) as well as the placements of the drawn regions/volumes of interest are shown in Supplemental Figure 1A.

SUV results were obtained first using PMOD's SUV image calculation scaler tool with a phantom measured weight of 0.073 kg. After scaling, a 2.8 mL VOI template was placed on the uniformity section of the PET IQ phantom for the extraction of SUV results. Representative image of VOI placement on the PET IQ phantom is shown in Supplemental Figure 1B. For analysis of variance an ordinary one-way (ANOVA) test was applied on the SUV data: default, standard and filter back projection (FBP).

PET spatial resolution assessment was conducted based on a visual assessment of the acquired images using the PET rod phantom. Horizontal profiles (H-profile) were drawn through

a center cross section, which included the largest rods (2 mm) obtained using the PMOD image profile tool.

CT. The phantoms were placed at the frontend of the scanner bed, positioned inside the bore at the isocenter, aligning sagittal, axial and coronal planes. For each default protocol, CT basic acquisition parameters varied by tube voltages (kVp), number of projections and exposure time (ms) by scanner as follows: 1 (40kVp, 360, 300ms), 2 (50kVp, 480, 300ms), 3 (80kVp, 220, 280ms), 4 (35kVp, 250, 300ms), and 5 (50kVp, 256, 555ms). CT protocol parameters per scanner are listed in Supplemental Table 3. All CT images were reconstructed with FBP.

CT Statistical analysis. Reconstructed CT data was imported into PMOD for analysis. A 5 mL VOI was placed on the air and water chamber of the CT air/water phantom to quantify the mean HU values (Supplemental Fig. 2A). The TEM phantom data was imported into PMOD and individually co-registered with an in-house developed TEM phantom template (Supplemental Fig. 2B), in order to ensure correct and consistent placement of VOIs on each rod for each CT image. A VOI template was generated for each rod (0.008 mL for 2 mm and 0.05 mL 4 mm) for extraction of HUs, (Supplemental Fig. 2B). HU quantification accuracy and precision was defined as bias between measured HU relative to established HU value for air, water and tissue, Table 1. The data is represented as the mean ±standard deviation (SD). Precision is assessed by measuring the SD and coefficient of variation (COV). For analysis of variance an ordinary one-way (ANOVA) test was applied on the TEM data, grouped per tissue density.

CT image spatial resolution was evaluated by visual assessment of the image obtained with the spatial resolution bar phantom. The number of structures (lines/dots with widths varying between 5 and 150 μm) on the bar pattern seen were compared to the manufacture's size chart to estimate each protocol spatial resolution.

Measurement of Ionizing Radiation Doses from CT Acquisition Protocols

An ionization chamber probe (10x6-0.6 CT Therapy QA Chamber, detection range 1μGy- 5kGy with ±4% calibration accuracy, Radcal, California, USA) was used for radiation dose measurements. The ion chamber probe was placed inside the CT dose index (CTDI) phantoms with the chamber in the center field of view (FOV). Default and standardized CT protocol measurements were obtained (n=3) on all scanners with the mouse and rat CTDI phantom.

The Radcal ion chamber software stops collecting/measuring at 300s. We previously showed the measured CT dose with the RadCal probe is linearly dependent on scan length (*21*). Therefore, CT protocols with a scan time longer than 5 minutes were measured to 300s then the dose was calculated based on remaining frames and measured dose, Equation 3.

$$\text{Measured CT dose} = \left(\frac{Frames_{protocol}}{Frames_{acquired}} \right) Dose_{measured} \quad \text{(Eq. 3)}$$

Standardized PET/CT Protocols

Developed standardized protocols were derived from the default protocol analysis results as described above and in Table 1. The actual PET and CT parameters available on each manufacture's scanner were also taken into consideration.

Standardizing the PET protocol entailed evaluating the impact different reconstruction methods had on the quantification of the PET image data sets. The following reconstruction algorithms were tested: FBP, OSEM with a combination of iterations*subsets of 12, 16, 24, 30, 32, 48 and 64 and MLEM with 12, 24, 25, 30, 32, 40 and 50 iterations. Quantitative analysis of the OSEM updates used in scanners 1, 2 and 3 revealed the optimal reconstruction methods were already being used for these particular scanners (Supplemental Table 4). For that reason, focus was placed on optimizing the MLEM method not only for improved accuracy but also for the best equivalent results to the OSEM method. Similarly, the MLEM method with 25 iterations

provided lower quantitative bias compared with OSEM outcomes from scanners 1-3. The FBP algorithm was deemed to be the optimal method for least quantitative bias across all scanners. Consequently, in the results section, we report data for scanner 1-3 default OSEM methods, scanner 4 and 5 default and standardized MLEM with 25 updates as well as FBP results for scanners 1-3 and 5.

From the analysis of the empirical CT data four standardized CT protocols were developed and tested. The tube voltage was set at 50 kVp and exposure time at 300 ms for all scanners with four varying number of projections (170, 360, 480 and 720 projections). Not all the scanners could set the projection parameters at 170 or 480. In those cases, data was only collected for the remaining protocols. CT collected data, including CT absorbed doses, were analyzed in the same manner as the default protocols, as outlined above. In the results section, CT imaging data derived from default and standard acquisition protocols using 360 projections are presented, given that all scanners allowed for this setting.

RESULTS

Analysis of PET Acquisitions using Default and Standardized Protocols

PET IQ. Seen in Fig. 1A, scanner 2 and 3 default reconstruction method overestimated the RCs by as much as 13% relative to 1 at the hot rod 3. Whereas, scanners 1, 4 and 5 default reconstruction method underestimated the RCs. The RCs measured for scanners 4 and 5 improved after implementing a standardized number of MLEM iterations at 25, shown in Fig. 1B. A 43% difference measured between scanner 3 and 4 at the 3 mm hot rod using default protocols was reduced to a 30% relative difference when using the standardized protocol. The FBP method produced the most consistent RCs of all methods (Fig. 1C).

Table 2 reveals poor image uniformity in scanner 5 before standardization. The standardized reconstruction protocol (MLEM 25) improved uniformity in scanner 5 by a relative

percentage difference of 36% (i.e. 16.7% to 10.6%). Though protocol standardization improved scanner 5's uniformity, there was no improvement in water and air SORs. This uniformity improvement was not observed in scanner 4 (MLEM 25), although its uniformity was already similar to OSEM data collected with other scanners. An improvement was seen in scanner 4's SORs for water and air. The mean uniformity value reduced by 12% when standardization was applied (improved coefficient of variation from 67% to 37%).

Analysis of the SUV variance proved significant for the default protocols and non-significant for the standard and FBP protocols (ANOVA: Default $p<0.001$, Standard $p<0.205$, FBP $p<0.388$ (FBP scanner 4 not included), n=3 per group). The greatest percentage difference (44%) in SUVs obtained using default protocols was between scanner 2 and 4. This was reduced to 14% with standardization. Using FBP, the greatest percent difference of 6% was measured between scanner 2 and 5. The percentage difference between the average expected SUV and the average default SUV or to the standardized SUV was 18% and 10%, respectively (Table 3 and Supplemental Fig. 3).

PET rod. Visual and horizontal profile analysis of the collected PET rod phantom data are shown in Supplemental Figure 4. Images reconstructed with the sites' default reconstruction methods showed the highest measured PET image resolution was 1.2 mm, as measured in scanner 3 and 5 (Supplemental Fig. 4A). When scanner 4 and 5 PET data were reconstructed using the standardized method 2.0 and 1.5 mm rods became well resolved in scanner 4, whilst scanner 5's spatial resolution remained essentially unchanged (Supplemental Fig. 4B).

Analysis of CT Acquisitions using Default and Standardized Protocols

CT air/water. The HU extracted using CT default acquisition protocols for scanners 2-4 were within a global average range for air of -989±13 HU (mean ± SD, n=3) and water 38±61 HU (mean ± SD, n=3). The greatest extracted HU for water was 133 HU and for air was -967 HU, measured in scanner 1.

When the standardized CT protocols were applied results for scanner 1 improved (water HU improved from 133 HU to -77HU), while HU water results for scanners 2-4 were all within ±30HU from 0HU (Table 4). The greatest measured HU for air when using CT standardized protocols was -990 HU.

CT TEM. A one-way ANOVA revealed significant differences across all tissue groups ($p<0.0001$, $n=3$), with the greatest variability (1581 HU, i.e. scanner means ranging between 3599 and 2018 HU) measured in the 1.57g/mL rod when CT default methods were used to collect imaging data (Fig. 2A). The HU values measured for the 1.08 g/mL TEM rod had a mean percentage difference of 90% when default CT protocols were used. Whilst the greatest mean percentage difference in the adipose rod was 147% between scanner 1 and 2. Two scanners showed the highest discrepancy in the HU comparison between the 4 mm and 2 mm rods of the same TEM (1.08 g/mL and 1.12 mg/mL hydroxyapatite). Scanner 1 calculated percentage difference between the 4 and 2 mm 1.08 g/mL hydroxyapatite rods was 130% and scanner 3 measured percentage difference between the 4 and 2 mm 1.12 g/mL hydroxyapatite rods was 158%.

The use of a CT standardized protocol improved quantitative precision for all the materials (Fig. 2B). The greatest improvement was measured in the rods with densities of 0.21, 0.95 and 1.08 g/mL representing lung, adipose and soft tissue, respectively. For example, the quantitative precision for the rod representing adipose tissue (0.95 g/mL) improved from a standard deviation of 77% with a coefficient of variation of 66% to a standard deviation of 22% and a coefficient of variation of 3% relative to the global mean. Furthermore, the lung rod measured a reduction of mean differences, in which scanner 3 improved from a mean of -728.4 HU, standard deviation of 35.16%, to a mean of -738.4 HU with a standard deviation of 0.64%. Also, the 1.57 g/mL hydroxyapatite rod's measured mean difference was reduced by 67% between scanners from 1581 to 518 HU. The large percentage difference seen in scanner 1 between 4 and 2 mm 1.08 g/mL rods when using default protocols reduced by 109% when

standardized protocols were used. However, in scanner 3, the measured percent difference between the 4 and 2 mm 1.12 g/mL hydroxyapatite rod was essentially unchanged.

CT Bar. Scanners 1, 2 and 4 were unable to resolve 150 μm lines using default protocols or distinguish the sections of lines/dots patterns. Scanner 5 had the highest spatial resolution for a default protocol of 150 μm (Supplemental Fig. 5A). A slight improvement (scanners 1-3) or no change in measured spatial resolution was seen when using the CT standardized protocol (Supplemental Fig. 5B).

Analysis of Measured Absorbed CT Radiation Dose using Default and Standardized Protocols

CT dose (CTDI). Measured CT absorbed doses using the default protocols at each site ranged from 11 mGy to 216 mGy (Table 5,). Ionizing radiation absorbed dose measurements in scanner 5 reduced by 81% when using the standard protocol. The absorbed CT doses measured was reduced by 48% (mouse phantom) and 40% (rat phantom) when using standardized CT protocols across sites.

DISCUSSION

We find the significant quantitative differences across routinely used default protocols concerning. For example, a commonly used analysis tool both in preclinical and clinical is the extractions of SUV measurements. An impacting factor on SUV measurements are the RCs and as shown the RCs greatly vary using different default reconstruction protocols. This is in line with previous reports on different PET reconstruction methods on image data quantification (*22–24*). Discordant SUV measurements are not only revealed across sites but internally between scanner's different reconstruction methods. Notably we measured a 54% difference in SUV for scanner 4 when changing from 12 MLEM to 25 MLEM. It was the FBP method that produced the most consistent and reproducible results across all scanners.

The literature spanning reconstruction methods (from FBP to iterative) is vast. Unfortunately, currently there is not a single solution that adequately fits all scanners due to differences in scanner manufacturing. The recently published paper by Mannheim et al. (2019) measured PET uniformity, RC and SOR in the Siemens Inveon and Focus using the reconstruction method of 2D OSEM 4*16. This method differs from both the various default reconstruction methods revealed and from the standardized protocol designed to suit all five different scanners in our study. Their study protocols in the Siemens platform produced similar uniformity and SOR but different RCs values from the five scanners (reconstruction methods) in our study (*16*) . This then begs the question of setting FBP as the standard for quantitative measurements given the improved precision of RCs and SUVs across sites. Nevertheless, using a combination of reconstructing with FBP and OSEM (as opposed to MLEM) serves the dual purpose of providing more accurate and precise quantitative information. The combined approach will also retain suitable image quality for better delineation of small organs and structures in preclinical animal species (*25*,*26*). Therefore, we recommend VOIs are drawn on the reconstructed OSEM image for better location/orientation then applied on the FBP image for accurate quantification. Based on our results, it is recommended that the total number of updates (iterations*subsets or iterations) are no less than 24 and no more than 36 for analysis of image data in conjunction with using FBP (Table 6).

Unlike PET, the CT image reconstructions were all done, default and standardized, with the FBP method. Though like PET the quantitative biases revealed with the default protocols were substantial. The significant variations in HU from the various CT default protocols reiterates the necessity of standardization. In this case the CT acquisition protocols have a more prominent role than reconstruction methods. Applying a standard CT acquisition protocol improved quantification precision of HU values across sites for each TEM measured as well as in air and water. The recommended standard CT protocol sets the tube voltage at 50 kVp for 300 ms with 360 projections (Table 6). This recommendation is completely feasible given that

every scanner enrolled in this study is capable of those parameters. However, it is important to emphasize the need for scanner calibration. Initially more than one scanner was plagued by calibration errors requiring intervention from the scanner manufacturer. Therefore, along with setting a CT protocol, correct calibration (HU values) at the different tube voltages needs to be ensured.

Furthermore, not until this study has the range of HUs values been measured at preclinical CT voltages.The traditional HU scale was established using clinical protocols with a higher tube voltage than 50 kVp (*27*). The average HU values we report here per TEM across multiple scanners can be used to establish preclinical HU ranges (Supplemental Table 5).

Our CT absorbed dose results indicate standardized protocols produce a reduction of the average absorbed ionized radiation received by small laboratory animals, with no image degradation. Unfortunately, the change in tube voltage to 50kVp in scanner 1 from 40kVp and scanner 4 from 35kVp with increased projections (250 to 360) led to an increase in the absorbed radiation dose. The amounts measured in the mouse and rat were increased by 77% and 86% in scanner 1. Scanner 4 measured an increase of 71% and 60% in the mouse and rat, respectively. However, even with the increase in scanner 1 and 4 all measured absorbed doses are now under limits of damaging ionizing radiation absorbed doses reported in the literature (<60mGy) (*13*,*18*,*28*,*29*). Critically, the measurements reported here provide a foundation for regulations regarding CT absorbed radiation doses. It should be noted that in the clinical setting absorbed radiation doses have been regulated since the 1950s (*30*). Implementing radiation dose regulations preclinically will therefore reduce cumulative severity, animal suffering while reducing the potential impact radiation may have on results especially in longitudinal studies.

CONCLUSION

Empirical PET and CT quantitative data variability reduces when standardized protocols are used. Adopting the suggested standardized protocol establishes continuity, allowing for

diagnostic and therapeutic agents to be developed and tested across imaging platforms with consistency. Data showed that standardization improves precision and accuracy in CT image quantification, while reducing the impact of absorbed ionizing radiation dose to small laboratory animals. Standardization will provided more robust, reliable and reproducible translational preclinical PET/CT imaging data sets. Therefore, this phantom work provides the foundational mainframe towards improving reproducibility of *in vivo* PET/CT measurements irrespective of scanner manufacture.

DISCLOSURE

All authors declare that they have no competing interests.

ACKNOWLEGMENTS

We thank the National Centre for the Replacement, Refinement and Reduction of Animals in Research (NC3Rs) for funding this work (Studentship grant NC/P00170X/1) to WM. AT is funded by the British Heart Foundation (RG/16/10/32375). The British Heart Foundation is greatly acknowledge for providing funding towards establishment of the Edinburgh Preclinical PET/CT laboratory (RE/13/3/30183). The authors would like to thank the radiochemistry teams at Edinburgh Imaging, Queen's Medical Research Institute (QMRI), the University of Aberdeen and Ghent University for their support in supplying the radiotracers used during the site visits.

KEY POINTS

QUESTION:

Will standardization of preclinical PET/CT protocols across multiple scanners reduce quantitative bias in image data while maintaining image quality?

PERTINENT FINDINGS:

Results unequivocally showed substantial and significant quantification bias across all scanners' when using each scanner default protocols on all CT and PET outcome measurements, including image quantification, resolution, uniformity, spill over ratios and absorbed dose. Developed and tested standardized preclinical PET/CT protocols improved accuracy and precision on all evaluations.

IMPLICATIONS FOR PATIENT CARE:

Implementing preclinical PET/CT standards produces more reliable and robust translational datasets, ultimately improving the success of clinical studies and applications.

REFERENCES

1. Smith WJM, Policy C, Schelbert HR, et al. Procedure guideline for tumor imaging using fluorine-18-FDG. *J Nucl Med*. 1998;39:1302-1305.
2. Young H, Baum R, Cremerius U, et al. Measurement of clinical and subclinical tumour response using [18F]- fluorodeoxyglucose and positron emission tomography: Review and 1999 EORTC recommendations. *Eur J Cancer*. 1999;35:1773-1782.
3. Boellaard R, Oyen WJG, Verzijlbergen FJ, et al. The Netherlands protocol for standardisation and quantification of FDG whole body PET studies in multi-centre trials. 2008:2320-2333.
4. Boellaard R, Doherty MJO, Weber WA, et al. FDG PET and PET / CT : EANM procedure guidelines for tumour PET imaging : version 1 . 0. 2010:181-200.
5. McGirr R, Hu S, Yee SP, Kovacs MS, Lee TY, Dhanvantari S. Towards PET imaging of intact pancreatic beta cell mass: A transgenic strategy. *Mol Imaging Biol*. 2011;13:962-972.
6. Palner M, Shen B, Jeon J, Lin J, Chin FT, Rao J. Preclinical kinetic analysis of the Caspase-3/7 PET tracer 18F-C-SNAT: quantifying the changes in blood flow and tumor retention after chemotherapy. *J Nucl Med*. 2015;56:1415-1421.
7. Massoud TF, Gambhir SS. Molecular imaging in living subjects: Seeing fundamental biological processes in a new light. *Genes Dev*. 2003;17:545-580.
8. Haylock AK, Spiegelberg D, Mortensen AC, et al. Evaluation of a novel type of imaging probe based on a recombinant bivalent mini-antibody construct for detection of CD44v6-expressing squamous cell carcinoma. *Int J Oncol*. 2016;48:461-470.
9. Zhang C, Pan J, Lin K-S, et al. Improved 68Ga-labelled truncated peptides targeting the neuropeptide Y1 receptor for cancer imaging by positron emission tomography. *J Nucl Med*. 2016;57:1160-1160.
10. Appelbe OK, Zhang Q, Pelizzari CA, Weichselbaum RR, Kron SJ. Image-guided

radiotherapy targets macromolecules through altering the tumor microenvironment. *Mol Pharm*. 2016;13:3457-3467.

11. Vanhove C, Bankstahl JP, Krämer SD, et al. Accurate molecular imaging of small animals taking into account animal models, handling, anaesthesia, quality control and imaging system performance. *EJNMMI Phys*. 2015;2:31.
12. Osborne DR, Kuntner C, Berr S, Stout D. Guidance for efficient small animal imaging quality control. *Mol Imaging Biol*. 2017;19:485-498.
13. Kersemans V, Thompson J, Cornelissen B, et al. Micro-CT for anatomic referencing in PET and SPECT: Radiation dose, biologic damage, and image quality. *J Nucl Med*. 2011;52:1827-1833.
14. Cavanaugh D, Johnson E, Price RE, Kurie J, Travis EL, Cody DD. In vivo respiratory-gated micro-CT imaging in small-animal oncology models. *Mol Imaging*. 2004;3:55-62.
15. Kuntner C, Stout D. Quantitative preclinical PET imaging: opportunities and challenges. *Front Phys*. 2014;2:1-12.
16. Mannheim JG, Mamach M, Reder S, et al. Reproducibility and comparability of preclinical PET imaging data: A multi-center small animal PET study. *Jounal Nucl Med*. 2019.
17. Mannheim JG, Kara F, Doorduin J, et al. Standardization of small animal imaging — current status and future prospects. *Mol Imaging Biol*. 2017;20:716-731.
18. Willekens I, Buls N, Lahoutte T, et al. Evaluation of the radiation dose in micro-CT with optimization of the scan protocol. *Contrast Media Mol Imaging*. 2010;5:201-207.
19. Szanda I, Mackewn J, Patay G, et al. National Electrical Manufacturers Association NU-4 performance evaluation of the PET component of the NanoPET/CT preclinical PET/CT scanner. *J Nucl Med*. 2011;52:1741-7.
20. Electrical N, Assocation M. NEMA Standards Publication NU 4 – 2008 Performance measurements of small animal positron emission tomographs. 2008.
21. McDougald WA, Collins R, Green M, Tavares AAS. High dose MicroCT does not

contribute toward improved MicroPET/CT image quantitative accuracy and can limit longitudinal scanning of small animals. *Front Phys*. 2017;5:1-11.

22. Ko H, Park S, Kim J, et al. A study on comparative analysis of SUVs before and after correction with use of recovery coefficient (RC) in partial volume effect (PVE). *Imaging Sci J*. 2014;62:11-15.
23. Srinivas SM, Dhurairaj T, Basu S, Bural G, Surti S, Alavi A. A recovery coefficient method for partial volume correction of PET images. *Ann Nucl Med*. 2009;23:341-348.
24. Soret M, Bacharach SL, Buvat I. Partial-volume effect in PET tumor imaging. *J Nucl Med*. 2007;48:932-945.
25. Qi J, Leahy RM, Cherry SR, Chatziioannou A, Farquhar TH. High-resolution 3D Bayesian image reconstruction using the microPET small-animal scanner. *Phys Med Biol*. 1998;43:1001-1013.
26. Qi J, Leahy RM. Iterative reconstruction techniques in emission computed tomography Iterative reconstruction techniques in emission. *Phys Med Biol*. 2006;51.
27. Schneider U, Pedroni E, Lomax A. The calibration of CT Hounsfield units for radiotherapy treatment planning. *Phys Med Biol*. 1996;41:111-24.
28. Carlson SK, Classic KL, Bender CE, Russell SJ. Small animal absorbed radiation dose from serial micro-computed tomography imaging. *Mol Imaging Biol*. 2007;9:78-82.
29. Foster WK, Ford NL. Investigating the effect of longitudinal micro-CT imaging on tumour growth in mice. *Phys Med Biol*. 2011;56:315-26.
30. Linet M. Historical Review of Cancer Risks in Medical Radiation Workers. 2014;174:793-808.

TABLES

Table 1. Criteria for quantitative analysis of PET and CT results.

PET			
PET IQ phantom	Uniformity	Recovery coefficients	Spill-out-ratio
	< 15%	1	< 0.20
Standard uptake value			
<10% bias			
CT	Hounsfield Units (HU) *		
CT Air/water phantom	Air	Water	
	0	-1000	
TEM phantom	Lung	Soft tissue (Adipose/muscle)	Bone (Soft/cortical)
	-700	>0	>200

Legend: * HU for TEM originally defined based on literature (*27*).

Table 2. PET IQ, measured uniformity and spill-over-ratios (SOR) using the default reconstruction methods and the standardized reconstruction method. Values expressed as mean±standard deviation, n=3.

	Default Protocol			Standardized Protocol		
Scanner	Uniformity (SD%)	SOR water	SOR air	Uniformity (SD%)	SOR water	SOR air
1	6.4±0.01	0.18±0.04	0.13±0.03	6.4±0.01	0.18±0.04	0.13±0.03
2	4.1±1.00	0.09±0.01	0.09±0.01	4.1±1.00	0.09±0.01	0.09±0.01
3	3.4±0.17	0.01±0.01	0.02±0.01	3.4±0.17	0.01±0.01	0.02±0.01
4	5.2±0.60	0.28±0.04	0.22±0.04	6.4±0.00	0.21±0.00	0.13±0.00
5	16.7±0.55	0.24±0.01	0.12±0.02	10.6±0.00	0.27±0.00	0.17±0.00

Table 3. Measured and expected standard uptake values (SUVs) for each scanner using the default, standardized reconstruction iterative method and FBP. Expected SUVs are measured from the dose calibrator and decay corrected. Measured SUVs are the mean SUV value extracted from PMOD. The "Average" SUV value per scanner is the averaged of the mean SUVs per site for n=3 measurements, expressed as mean±standard deviation. SUV data is also presented as normalized to the mean SUV measurement per scanner.

Scanner	Expected	Default	Measured/ mean	Standard	Measured /mean	FBP	Measured/ mean
Scanner 1	3.61±0.59	3.24±0.34	1.04±0.11	3.24±0.34	0.96±0.09	3.26±0.14	1.03±0.04
Scanner 2	3.87±0.62	3.77±1.06	1.21±0.34	3.77±1.06	1.12±0.31	3.18±0.39	1.00±0.12
Scanner 3	4.11±0.12	3.63±0.19	1.17±0.06	3.63±0.19	1.08±0.05	3.29±0.17	1.04±0.05
Scanner 4	3.64±0.31	2.10±0.07	0.68±0.00	3.24±0.01	0.96±0.00	NA	NA
Scanner 5	3.52±1.12	2.82±0.15	0.91±0.05	2.93±0.46	0.87±0.13	2.98±0.02	0.94±0.00

Legend: NA=not available, FBP=filtered back projection. ANOVA: Default $p<0.001$, Standard $p<0.205$, FBP $p<0.388$ (FBP scanner 4 not included), n=3 per group.

Table 4. Hounsfield Units (HU) measured using the CT air/water phantom and default/standardized protocols. Results presented as the average (Ave) and standard deviation (STDEV) of HUs for each scanner (n=3). The standardized protocol could be acquired for scanner 4 but could not be quantified as the scanner vendor could not make available calibration files for the tube voltage used. Scanner 5 is not calibrated to measure HU values; output results are a linear gray scale. Scanner 5 HU conversion results are displayed on the bottom.

Scanner	Ave HU Water (0)	Water STDEV	Ave HU Air (-1000)	Air STDEV
1 Default	133.05±5.94	284.35±4.07	-967.86±5.35	149.97±0.73
Standardized	-77.91±1.15	122.32±35.89	-990.46±2.72	82.21±19.61
2 Default	-29.62±0.49	32.28±0.08	-993.54±0.08	11.34±11.30
Standardized	-27.88±0.40	35.59±0.10	-993.29±0.05	12.06±0.13
3 Default	16.97±3.68	43.18±0.10	-994.98±0.61	15.76±6.10
Standardized	28.78±2.33	45.95±0.081	-996.92±0.08	7.15±0.10
4 Default	24.85±6.77	24.42±1.05	-1000±0.00	8.85E-12
Scanner 5 not calibrated to measure HU (output in linear gray scale)				
Scanner 5 converted to HU				
5 Default	-10.12	64.9	-1008.26	92.03
Standardized	-3.42	142.52	-1024.19	73.47

Table 5. CT absorbed doses determined using default protocols and a standardized protocol for mice and rats. Results expressed as mean±standard deviation, n=3.

	Default (mGy)		Standard (mGy)		Measured dose difference default to standard (%)	
Scanner	Mouse	Rat	Mouse	Rat	Mouse	Rat
1	11±0.10	7±0.10	20±0.09	13±0.16	+77	+86
2	40±0.11	28±0.02	31±0.23	21±0.08	-23	-23
3	59±0.03	48±0.11	39±0.23	28±0.08	-34	-42
4	32±0.18	15±0.10	56±0.76	25±0.05	+71	+60
5	216±0.02	100±0.17	41±0.02	31±0.03	-81	-69

Table 6. Proposed preclinical standard protocols for daily routine use irrespective of scanner/site.

PET reconstruction: Iterative algorithms OSEM or MLEM total updates (iterations*subsets or iterations) to be in the range of 24 to 36. FBP is also recommended for use in conjunction with iterative methods.
CT image acquisition parameters for FBP reconstruction methods: Tube voltage at 50 kVp Number of projections at 360 Exposer of 300 ms

FIGURES

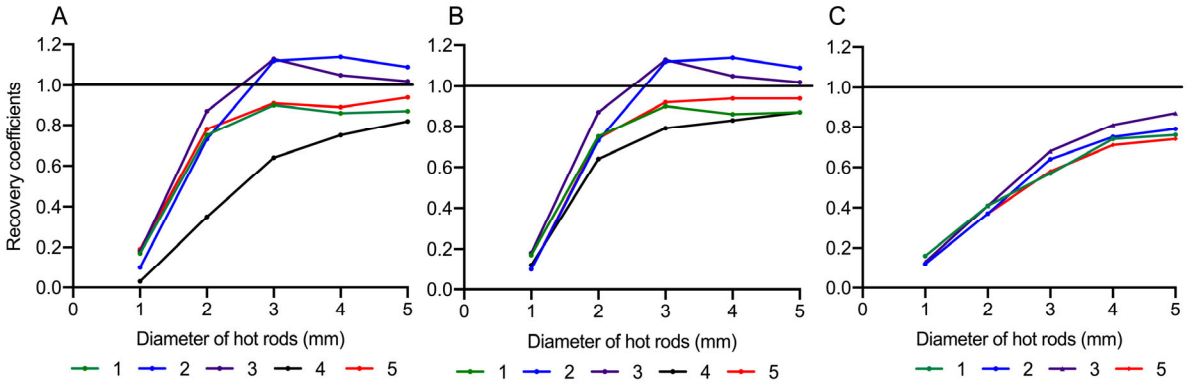

Figure 1. Recovery coefficients (RCs) for hot rods of 1, 2, 3, 4 and 5 mm of the PET IQ phantom extracted for each scanner. Panel (A): default reconstruction methods for scanners 1 (2D OSEM 2 iterations 16 subsets), 2 (3D OSEM 4 iterations 6 subsets, PSF), 3 (3D OSEM 2 iterations 18 subsets, PSF), 4 (3D MLEM 12 iterations), 5 (2D MLEM 50 iterations). Panel (B): displays RCs with standardization for scanner 4 (3D MLEM 25) and scanner 5 (2D MLEM 25) leaving scanners 1, 2 and 3 with the default reconstruction method. Panel (C): RCs for each site using FBP reconstruction with the exception of scanner 4 (reconstruction option not available yet).

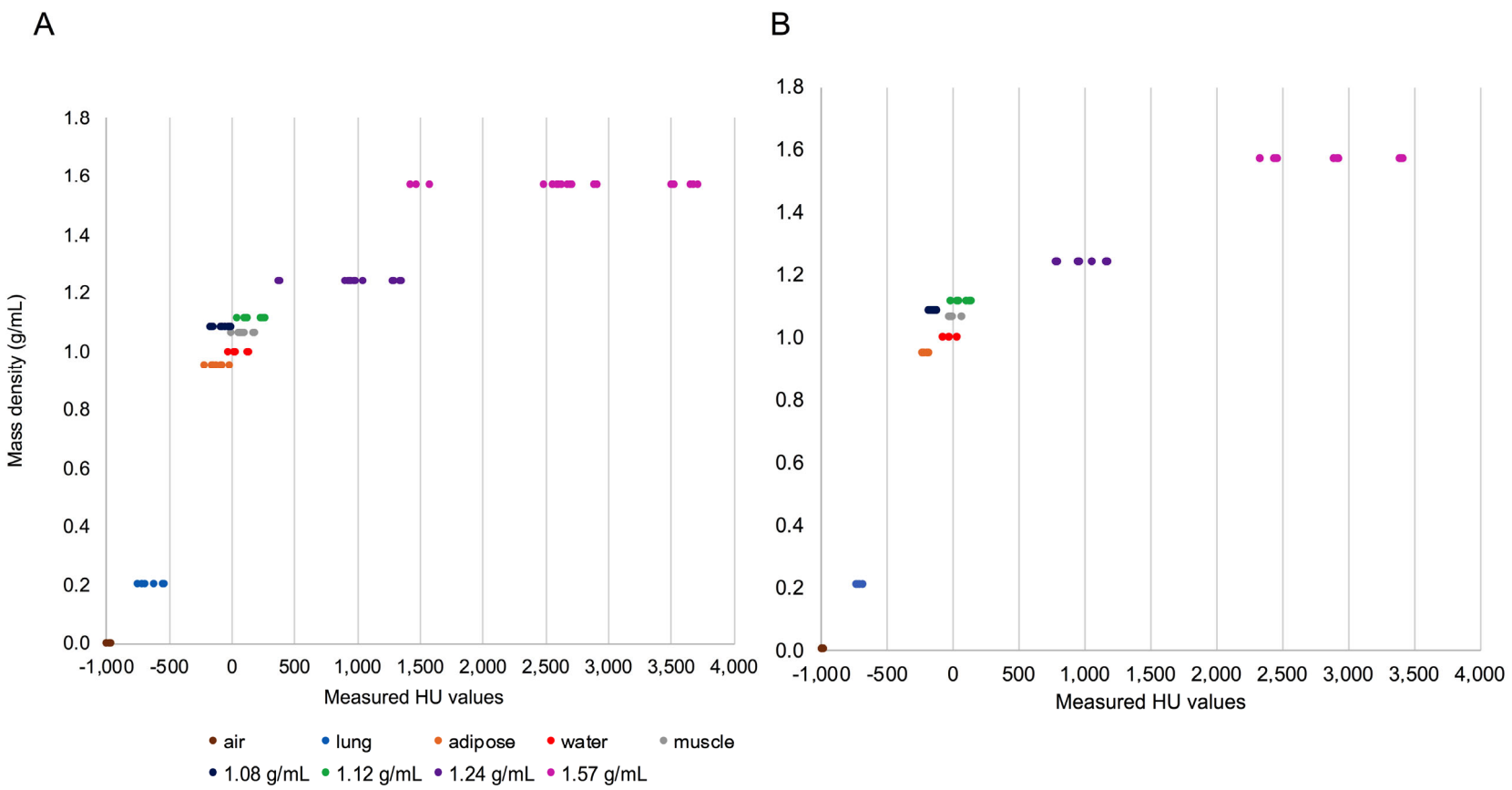

Figure 2. CT TEM, air and water HU results. For each material, each data point represents a measurement from a scanner (n=3) from four different sites. Densities 1.08 to 1.57 g/mL include rod sizes 2 mm and 4 mm as reported by the manufacturer. The x-axis clearly shows the spread of HU values per density (A) and displays the significant variations measured using the default protocols ($p<0.0001$, one-way ANOVA, n=3 per group). (B) Improved precision across scanners and densities when using the standardized protocol.

Supplemental Data

Supplemental Table 1. Scanner parameters and NEMA NU4-2008 testing results derived from literature, (*1–13*)

Scanner	Scintillator	Coincidence timing (ns)	Ring diameter (cm)	Axial FOV (cm)	Crystal size (mm)	Number of detector modules	Detector	Peak sensitivity (%)	Resolution/ crystal size
Bruker Albira	LYSO	5	10.5	14.8	50 x 50 x 10	24	3 ring SiPM	5.3	< 2.0
Mediso nanoPET/CT	LYSO:Ce	5	18.1	9.48	1.12 x 1.12 x 13	12	1 ring PMT	7.7	< 2.5
Sedecal Super Argus	LYSO & GSO	5	11.8	4.8	1.45 x 1.45x 15	36	2 ring PMT	4.32	1.14
Siemens Inveon	LSO	3.4	16.1	12.7	1.51 x 1.51 x10	16	PMT	6.72	1.08
Trifoil LabPET/CT	LYSO & LGSO	22	16.2	7.5	2 x 2 x 12	768	APD	2.36	0.82

Supplemental Table 2. Summary of microPET/CT commercial phantoms used in this study at each site.

Phantoms	Size	Brief description	Measurement
microPET			
A: PET Image Quality (IQ), Bartec: PH-60-00-50	8 x 3.5cm	Three chambers: (chamber 1) two 8mm cylinders, (chamber 2) central uniform region and (chamber 3) five rods with varying diameters of 1, 2, 3, 4, and 5mm	Spill over ratio, uniformity and recovery coefficients
B: microPET rod, QRM: MicroPET HotRod	7 x 3.5cm	Set of 6 triangular patterns with rods varying in diameter (0.6, 0.8, 1.0.1.2, 1.5 and 2.0mm)	Spatial resolution
microCT			
C: Air/water Quality Control (QC), Bartec: PH-60-00-60	6.5 x 3cm	Dual chamber air and water	Accuracy of air and water Hounsfield Units (HU)
D: Tissue Equivalent Material (TEM), CIRS: MicroCT rods 091	9.5 x 3cm	Rods (2 to 5mm) of polymer materials representing lung, muscle, adipose tissue, and hydroxyapatite (0, 50, 250 & 750 mg/ml)	Hounsfield Units (HU) for equivalent/representative tissues
E: CT bar, QRM: MicroCT Barpattern-NANO	4 x 2cm	Chip with bar and circle patterns ranging from 5 to 150μm in thickness and diameter, respectively	Spatial resolution
F: Mouse CT Dose Index (CTDI), Bartec: PH-60-00-05	15 x 3cm	Cylinder with central bore - for ion chamber	Dose Index (radiation delivered)
G: Rat CT Dose Index (CTDI), Bartec: PH-60-00-06	15 x 6cm	Cylinder with central bore - for ion chamber	Dose Index (radiation delivered)

(A)

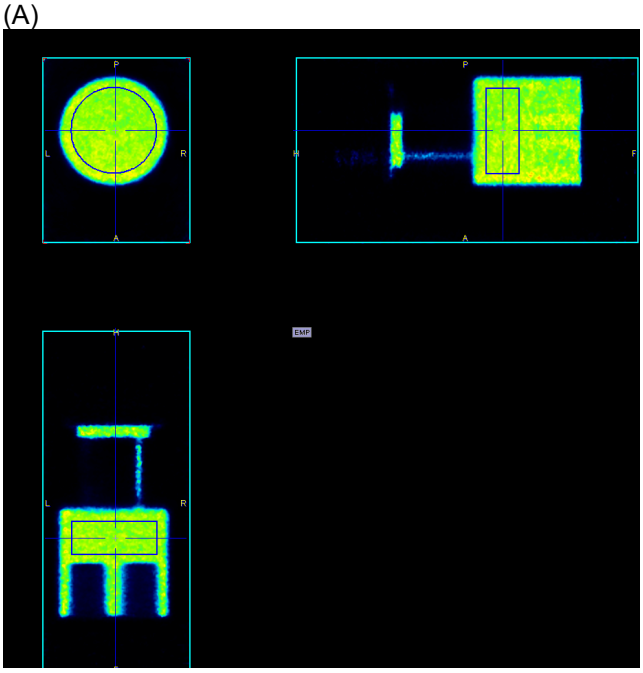

(B)

ROI for uniformity ROI for recovery coefficient ROI for water and air spill-out-ratio

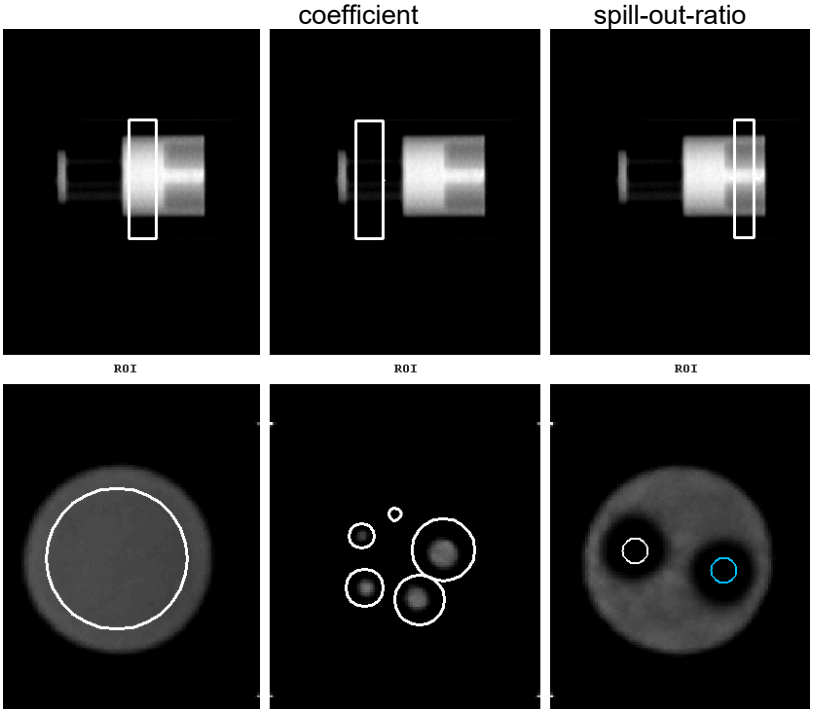

Supplemental Figure 1. (A) PMOD screen shot showing the VOI placement on the PET IQ uniformity region for SUV measurements. (B) Screen shot of the Mediso's MATLAB software tool for the PET IQ analysis displaying the regions of the IQ phantom (uniformity, RC and SOR) as well as the placements of the regions.

Supplemental Table 3. Summary of site's/scanner's CT default protocols evaluated. Scan duration (s) recorded from CT dose measurements (n=3).

Scanner	Scan method	Number projections	Tube voltage (kVp)	Exposure time (ms)	Scan duration (s)	Binning	Zoom	Focal spot (µm)	Current (µA)
1	circular	360	40	300	130.90	1:1	none	35	140
2	circular	480	50	300	166.80	1:4	max FOV	33	520
3	step-in-shoot	220	80	280	236.30	1:4	low	< 6	500
4	circular	250	35	300	277.70	1:4	none	35	200
5	circular	256	50	555	323.83	1:1	low	33	760

(A)

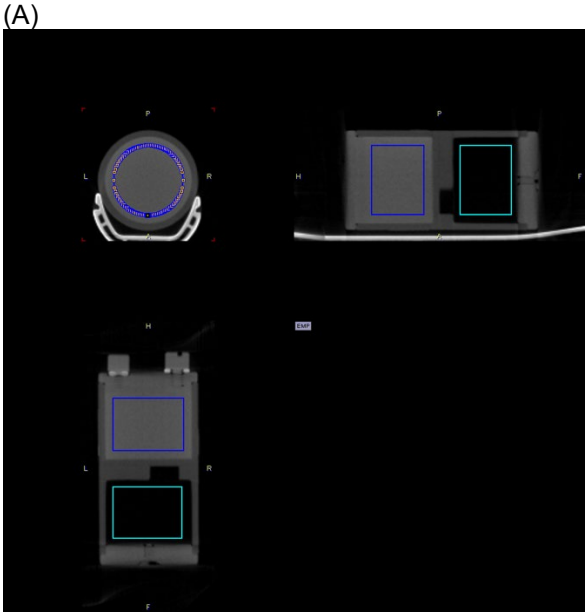

(B)

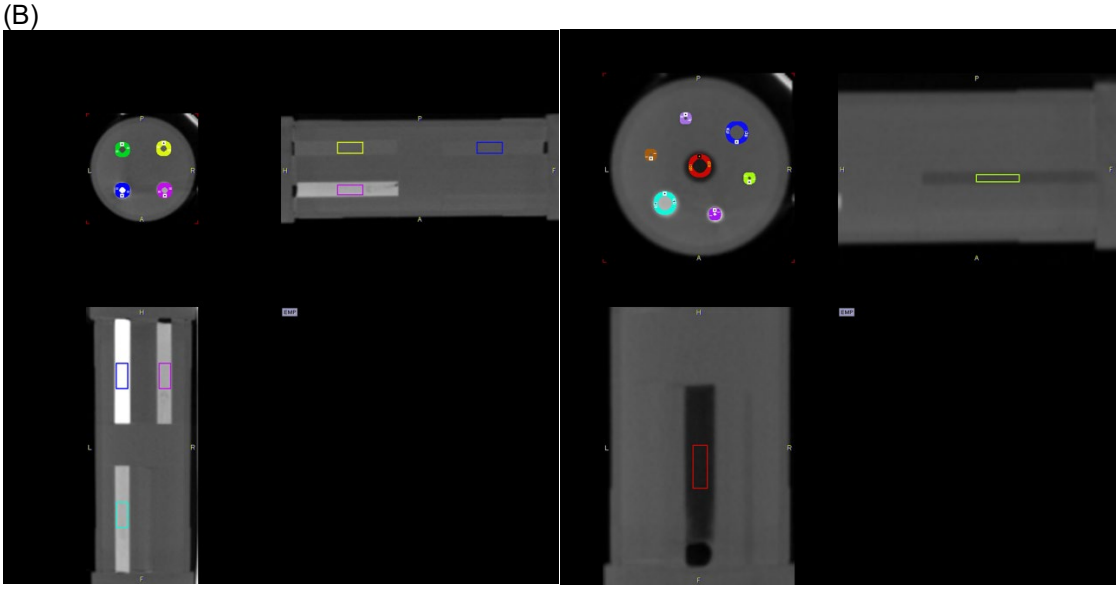

Supplemental Figure 2. (A) PMOD screen shot showing the VOI placement on the CT water and air region for HU measurements. (B) PMOD screen shot showing the VOI placement on the CT TEM phantom rods for HU measurements.

Supplemental Table 4. PET IQ data analysis showing uniformity, RC and SOR for each scanner for the default and additional reconstruction methods. Sections are divided by scanners (1-5) in which rows indicate the reconstruction method used and the data analysis results per column heading.

	Reconstruction (updates)	Uniformity (SD%)	RC (1mm)	RC (2mm)	RC (3mm)	RC (4mm)	RC (5mm)	Water SOR	Air SOR
Scanner 1	OSEM								
	24	5.4	0.14	0.67	0.86	0.87	0.87	0.17	0.14
default	32	6.4	0.17	0.75	0.90	0.86	0.87	0.18	0.13
	64	9.2	0.21	0.82	0.85	0.82	0.86	0.17	0.11
	FBP	11.3	0.16	0.41	0.57	0.74	0.76	0.21	0.13
Scanner 2	OSEM								
	12	4.6	0.05	0.40	0.93	1.04	1.09	0.11	0.10
default	24	4.1	0.10	0.73	1.12	1.14	1.09	0.09	0.09
	30	4.6	0.22	0.79	1.17	1.06	1.20	0.09	0.09
	32	4.7	0.13	0.79	1.13	1.06	1.04	0.08	0.10
	36	4.9	0.19	0.77	1.14	1.15	1.09	0.07	0.06
	48	4.4	0.18	0.76	1.16	1.17	1.10	0.07	0.07
	FBP	10.9	0.12	0.37	0.64	0.75	0.79	0.11	0.08
Scanner 3	OSEM								
	12	2.7	0.11	0.84	1.24	1.11	1.02	0.03	0.02
	24	3.2	0.18	0.92	1.17	1.03	1.05	0.02	0.02
	32	3.3	0.19	0.91	1.14	0.98	1.05	0.02	0.02
default	36	3.4	0.18	0.87	1.13	1.05	1.02	0.01	0.02
	64	3.7	0.19	0.88	1.14	1.00	1.04	0.03	0.02
	FBP	4.3	0.13	0.41	0.68	0.81	0.87	0.01	0.01
Scanner 4	MLEM								
default	12	5.2	0.03	0.35	0.64	0.75	0.82	0.28	0.22
	24	4.5	0.09	0.49	0.68	0.79	0.85	0.22	0.13
	25	6.4	0.12	0.64	0.79	0.83	0.87	0.21	0.13
	30	5.1	0.11	0.51	0.68	0.79	0.85	0.21	0.11
	32	6.7	0.12	0.54	0.69	0.78	0.86	0.20	0.12
	40	9.4	0.16	0.68	0.76	0.81	0.88	0.16	0.08

	50	11.70	0.18	0.66	0.74	0.81	0.88	0.18	0.08
Scanner 5	MLEM								
	12	6.7	0.05	0.45	0.82	0.92	0.96	0.33	0.25
	24	12.4	0.11	0.79	0.92	0.93	0.94	0.25	0.13
	25	10.6	0.10	0.74	0.92	0.94	0.94	0.27	0.17
	30	11.9	0.11	0.78	0.92	0.93	0.94	0.26	0.16
	32	12.1	0.11	0.79	0.92	0.91	0.93	0.24	0.13
	40	14.1	0.13	0.82	0.91	0.91	0.95	0.25	0.14
default	50	16.7	0.19	0.78	0.91	0.89	0.94	0.24	0.12
	FBP	20.8	0.12	0.37	0.58	0.71	0.74	0.24	0.06

As seen in scanner 1; reconstruction methods (updates) limited by scanner's parameters.

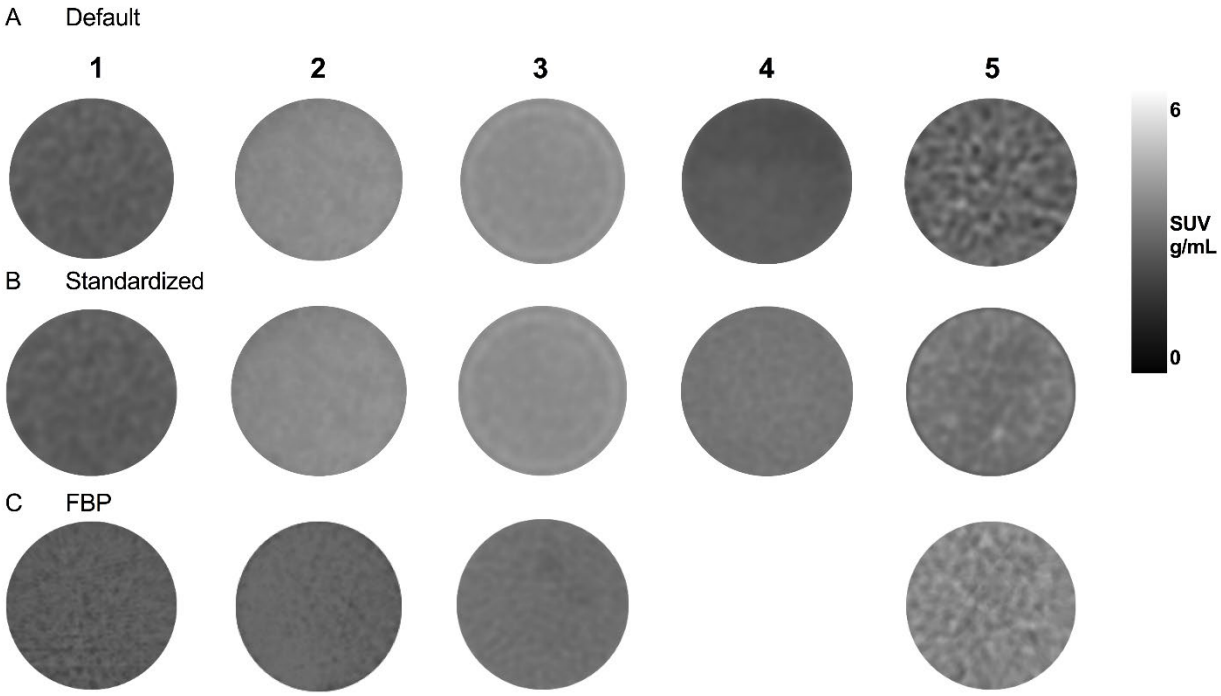

Supplemental Figure 3. Image slice through the uniformity section of the PET IQ phantom for each scanner shows variability in scanner uniformity as well as SUV measurements when using the scanner default and varying reconstruction protocols. Panel (A) shows the default, panel (B) the standard and panel (C) displays the FBP reconstruction method.

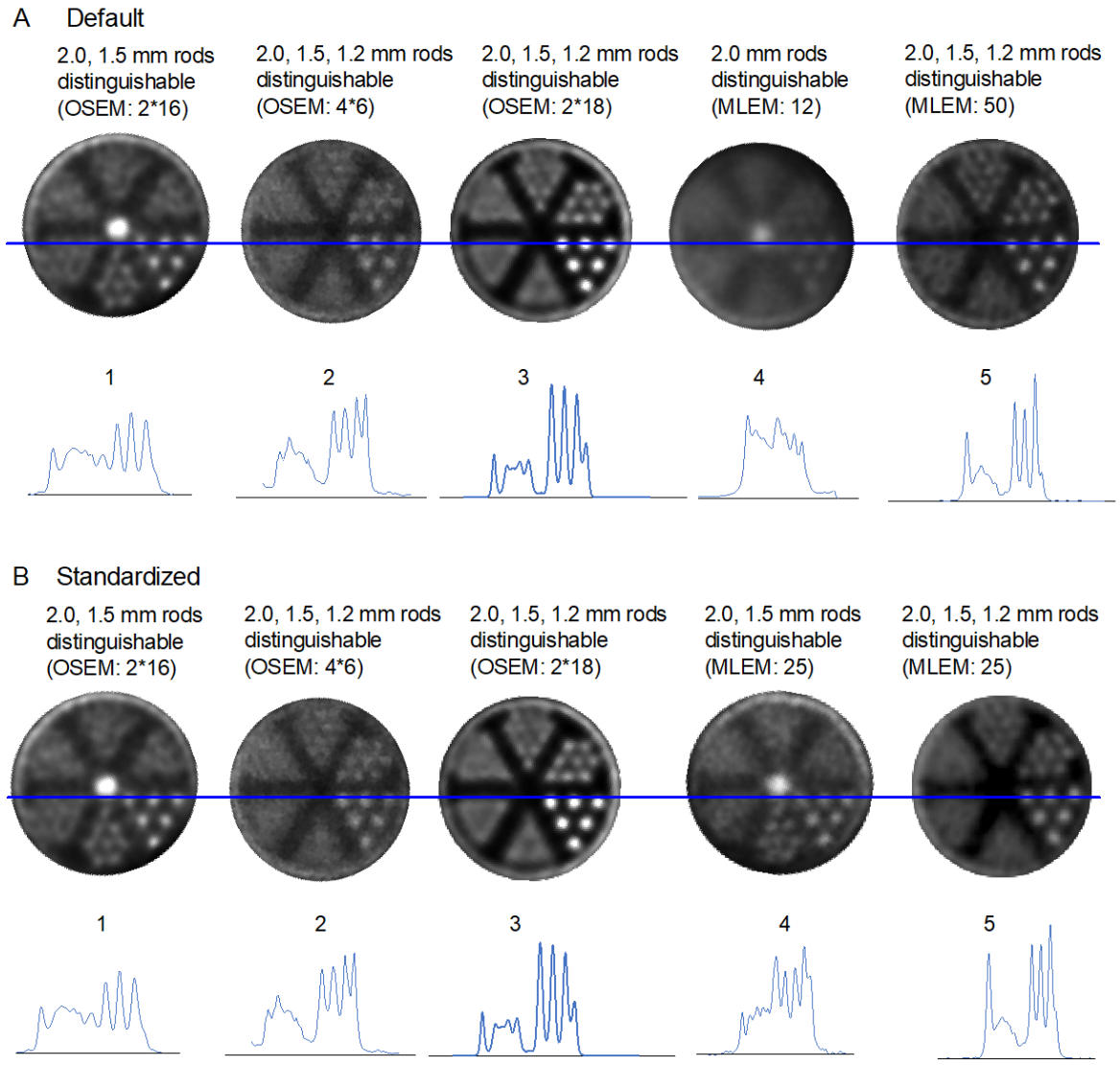

Supplemental Figure 4. Image slice and horizontal profile through the PET rod phantom. Panel (A): Scanners 2, 3 and 5 resolved 2.0, 1.5 and 1.2 mm rods using default reconstruction protocols. Panel (B): Standardized reconstruction methods improved the spatial resolution of scanner 4 (2.0 and 1.5 mm rods are seen) and essentially did not change the spatial resolution of scanner 5.

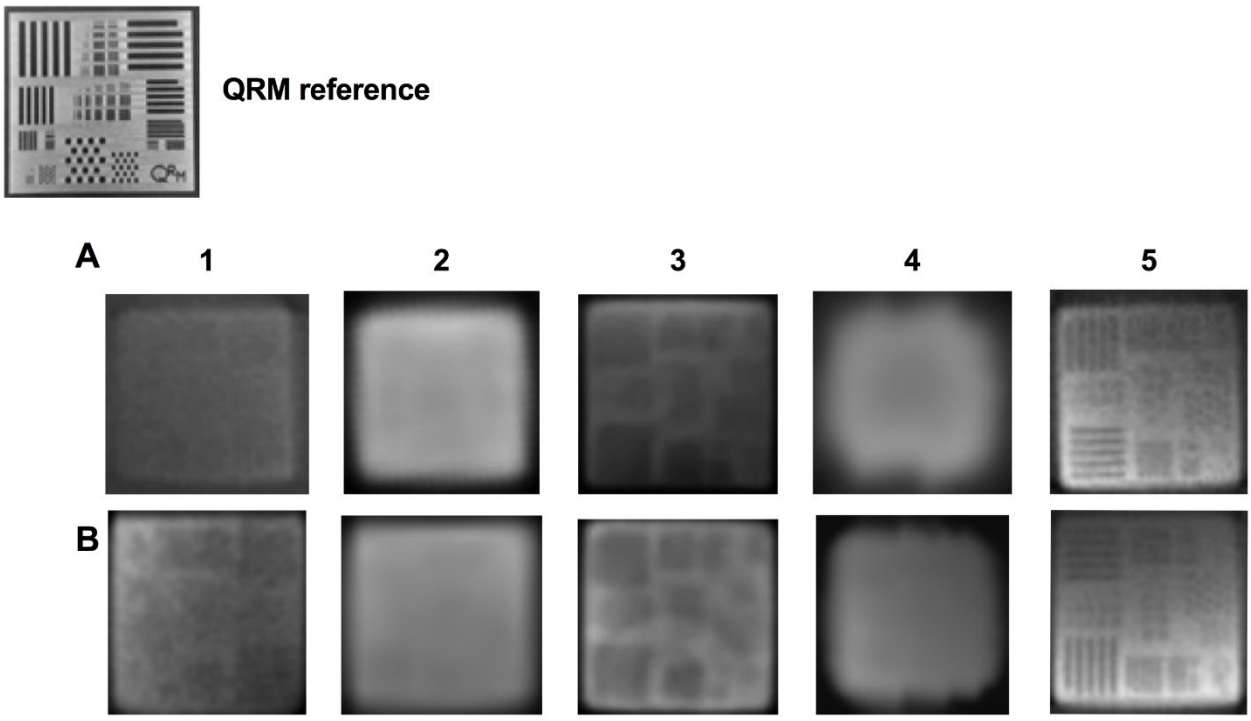

Supplemental Figure 5. CT bar phantom images displaying QRM pattern for spatial resolution using the default (A) and post standardization (B) of CT protocols.

Supplemental Table 5. Proposed preclinical Hounsfield Unit (HU) range generated using the standard CT protocol (tube voltage at 50 kVp, 300 ms and 360 projections) and the tissue equivalent material phantom. Soft tissue and bone HUs are averaged using the 2mm and 4mm rods.

Lung range	-778	to	-686
Adipose range	-233	to	-177
Muscle range	-8	to	64
Soft tissue range (0.95 to 1.115 g/mL)	-204	to	74
Bone range (1.24 to 1.57 g/mL)	987	to	2900

References:

1. Nagy K, Toth M, Major P, et al. Performance Evaluation of the Small-Animal nanoScan PET/MRI System. *J Nucl Med*. 2013;54:1825-32.
2. Goertzen a. L, Bao Q, Bergeron M, et al. NEMA NU 4-2008 Comparison of Preclinical PET Imaging Systems. *J Nucl Med*. 2012;53:1300-1309.
3. Constantinescu C, Mukherjee J. NIH Public Access. *Phys Med Biol*. 2009;54:2885-2899.
4. Bergeron M, Member S, Cadorette J, et al. Performance Evaluation of the LabPET APD-Based Digital PET Scanner. *IEEE Trans Nuc Sci*. 2009;56:10-16.
5. Canadas M, Sanz E, Vives M, et al. Performance Evaluation for 68Ga and 18F of the ARGUS Small-Animal PET Scanner Based on the NEMA NU-4 Standard. *IEEE Nucl Sci Symp Conf Rec*. 2010.
6. Disselhorst J a, Brom M, Laverman P, et al. Image-quality assessment for several positron emitters using the NEMA NU 4-2008 standards in the Siemens Inveon small-animal PET scanner. *J Nucl Med*. 2010;51:610-617.
7. Szanda I, Mackewn J, Patay G, et al. National Electrical Manufacturers Association NU-4 performance evaluation of the PET component of the NanoPET/CT preclinical PET/CT scanner. *J Nucl Med*. 2011;52:1741-7.
8. Bao Q, Newport D, Chen M, Stout DB, Chatziioannou AF. Performance evaluation of the inveon dedicated PET preclinical tomograph based on the NEMA NU-4 standards. *J Nucl Med*. 2009;50:401-408.
9. Pajak MZ, Volgyes D, Pimlott SL, et al. NEMA NU4-2008 Performance Evaluation of Albira : A Two-Ring Small-Animal PET System Using Continuous LYSO Crystals. 2016.
10. Herrmann K, Dahlbom M, Nathanson D, et al. Evaluation of the Genisys4, a Bench-Top Preclinical PET Scanner. *Nucl Med*. 2013;54:1162-1167.
11. Tai Y, Ruangma A, Rowland D, et al. Performance evaluation of the microPET focus: a third-generation microPET scanner dedicated to animal imaging. *J Nucl Med*. 2005;46:455-63.
12. Kis SA, Valastyán I, Hegyesi G, et al. Performance Characteristics of a miniPET Scanner Dedicated to Small Animal Imaging. In: IEEE Nuclear Science Symposium Conference Record. Vol 3. ; 2005:1645-1648.
13. Yang Y, Tai Y-C, Siegel S, et al. Optimization and performance evaluation of the microPET II scanner for in vivo small-animal imaging. *Phys Med Biol*. 2004;49:2527-2545.

The Journal of NUCLEAR MEDICINE

Standardization of preclinical PET/CT imaging to improve quantitative accuracy, precision and reproducibility: a multi-center study

Wendy McDougald, Christian Vanhove, Adrienne Lehnert, Barbara Lewellen, John Wright, Marco Mingarelli, Carlos Corral, Jurgen Schneider, Sven Plein, David Newby, Andy Welch, Robert Miyaoka, Stefaan Vandenberghe and Adriana A. S. Tavares

J Nucl Med.
Published online: September 27, 2019.
Doi: 10.2967/jnumed.119.231308

The Journal of Nuclear Medicine is published monthly.
SNMMI | Society of Nuclear Medicine and Molecular Imaging
1850 Samuel Morse Drive, Reston, VA 20190.
(Print ISSN: 0161-5505, Online ISSN: 2159-662X)

SNMMI SOCIETY OF NUCLEAR MEDICINE AND MOLECULAR IMAGING